Radiocarbon measurement of CO₂ from carbonate minerals using a hybrid gas ion source with an open split interface

Brett E. Longworth^a, Joshua R. Burton^a, Simon L. Pendleton^{a,b}, Sydney D. Moser^c, Mark L. Roberts^a, Mark D. Kurz^a

^aDepartment of Geology and Geophysics 360 Woods Hole Rd. Woods Hole MA 02540
^bEnvironmental Science and Policy 17 High St. Plymouth NH 03264
^cGeography Environment and Geomatics 550 Cumberland St. Ottawa ON Canada K1N 6N5

Abstract

We have developed a method for measuring radiocarbon in carbonate minerals as CO_2 gas via a NEC MCSNICS hybrid sputter gas ion source (HGIS). The method uses helium as a carrier gas to displace CO_2 from sample vials to an open split, where a glass capillary samples the mixture for delivery directly to the HGIS. This method skips the gas transfer and quantification steps used in a closed inlet HGIS system, simplifying sample measurement. Samples larger than 8 mg carbonate can be measured. Results from measurements of consensus standards (TIRI I, IAEA C2, and an internal modern shell standard), and samples from a marine core ($F^{14}C = 0.4$ –1.15) show that the method agrees well with traditional AMS measurement of the same samples as graphite, and that the 1σ uncertainty is about 1%. We discuss advantages and disadvantages of continuous flow sample introduction, and the effect of reduced precision on calibrated age-depth models produced using gas-source data.

Keywords: radiocarbon, carbonate, hybrid gas ion source

^{*}Corresponding author

Email addresses: blongworth@whoi.edu (Brett E. Longworth), jburton@whoi.edu (Joshua R. Burton), simon.pendleton@plymouth.edu (Simon L. Pendleton), smose007@uottawa.ca (Sydney D. Moser), mroberts@whoi.edu (Mark L. Roberts), mkurz@whoi.edu (Mark D. Kurz)

1. Introduction

Radiocarbon Accelerator Mass Spectrometry (AMS) is a sensitive method for determining the age, provenance, and composition of carbon-containing materials. A primary disadvantage of the method is cost, which can limit the number of samples analyzed. This forces researchers to carefully select samples for analysis and may limit repeat measurements for error determination. One driver of the cost of AMS analysis is the time and effort required for sample preparation, including reduction of the sample to graphite. Analysis of CO₂ directly via a gas-accepting AMS ion source eliminates the cost and effort of graphitization and returns results more rapidly. The NOSAMS USAMS system at the National Oceanographic AMS lab (NOSAMS) is based on a 3MV Tandetron accelerator [1] combined with a National Electrostatics Corporation (NEC) 134-sample gas-capable MCSNICS source. The hybrid gas capability of this source was developed as a joint project between NEC and the Scottish Universities Environmental Research Centre (SUERC) [2], and further improved by work at Lawrence Livermore National Laboratory (LLNL) [3]. We present here a system for semi-automated analysis of carbonate minerals by acid hydrolysis in vials and introduction to the ion source in a flow of helium via an open split, and results for measurements of reference materials and shell macrofossils from a marine sediment core.

Most interfaces to gas-accepting sputter ion sources are a closed inlet design [2,4-9]. A mixture of sample and helium is introduced to the source through a capillary, and flow is controlled by the pressure in the inlet volume and the length and diameter of the capillary. Pressure is adjusted by changing either the inlet volume or the amount of gas in the inlet. We designed a open inlet where a capillary samples gas for delivery to the ion source in a flowing stream that exhausts to the atmosphere, referred to here as an open split. This defines the delivery pressure as 1 ATM. CO_2 flow to the source can be controlled by changing the length or diameter of the capillary, or by changing the ratio of CO_2 to He in the sample stream.

An open inlet has the advantage of simplicity; flow of gas to the source is preset by capillary parameters and there are no separate sample transfer and dilution steps. This may translate to greater throughput by eliminating the time required for sample transfer, dilution, and setting of delivery pressure. Reduced system complexity also minimizes points of failure and eases automation and maintenance.

A disadvantage of the open split is that the flow of CO_2 to the source varies with sample size (CO_2 :He) and changes over the course of a measurement due to dilution of the sample by displacement helium. Our method compensates for this by limiting CO_2 flow to a range that produces relatively constant $^{12}C^{-}$ ion current and stable ratios. In gas-source AMS, Roberts et al. [10] used an open split to introduce sample gas to a ECR ion source and Salazar and Szidat [11] designed a continuous flow system that maintains relatively stable pCO_2 during acquisition by controlling pressure and venting excess gas to atmosphere.

The gas-capable 134-sample MCSNICS from National Electrostatics Corporation (NEC) [2] works on the same principle as hybrid sources developed by ETH Zürich [5,12] and High Voltage Engineering Europa (HVEE) [13]. The sample CO_2 - helium mixture is introduced onto a titanium insert or frit in an aluminum target cathode using stainless tubing mounted to an arm with a probe that mates with the back of the cathode. Sample gas is exposed to a beam of charged cesium atoms as it flows over the titanium insert, which causes dissociation of CO_2 and ionization of molecular and atomic species. Negative ions are extracted from the target, carbon species are selected, and interfering masses filtered out by the USAMS Tandetron beamline.

2. Method

2.1. Inlet description

The open split interface (Figure 1) supplies a CO_2 - helium mixture to a split where a capillary transfers gas to the ion source and the gas not taken by the capillary is vented. Flowing helium is used to displace sample CO_2 from the sample vial to the delivery capillary in the split. The open-split interface is constructed of simple, off-the-shelf parts. The core of the design is a dual needle and split housed in a Valco tee fitting. Displacement helium flows in through the sidearm of the tee and into the sample vial through 1/16 in stainless steel tubing, which forms the outer flow path of the concentric dual needle.

The mixture of sample CO_2 and displacement helium from the vial flows up a 21 gauge (0.819 mm) needle inserted through the tee and stainless tubing which forms the inner flow path of the dual needle. The open split is a VICI Luer adapter (part ZBUMLPK) with 5 cm of 1/16 in. PFTE tubing attached. The split is connected to the top of the inner needle, and the source delivery capillary is inserted into the split. The split has fairly low volume (< 1 mL). The system was operated manually during development but could be mounted on the arm of a vial-sampling autosampler to enable automated operation. The dual needle and open split design are similar to those used by Roberts et al. [10], with the differences that helium, rather than water, is used for sample displacement, and displacement helium flows into the vial through the outer/upper flow path.

The helium displacement flow rate was set to 250 μ l min⁻¹ for initial tests, and this was reduced to 100 μ l min⁻¹ for later work, including most reference standard comparisons and the core comparison. The flow rate from the open split into the source was defined by 150 cm of 50 μ m diameter fused silica capillary, split into two sections by a zero-volume bulkhead connector at the source high-voltage cage. The section inside the cage was jacketed in 1/16 in. PFTE tubing to help protect against spark damage. The total flow rate of gas to the source varied between 30 μ l min⁻¹ for pure helium and 40 μ l min⁻¹ for pure CO₂ due to the viscosity difference between helium and CO₂, estimated using the Hagen-Poiseuille equation. The HGIS itself is as described by Xu et al. [Xu2007].

2.2. Sample preparation

Carbonate samples were weighed into 7 ml septa-sealed glass vials (Labco 768W). Sealed vials were evacuated, then 1 ml 85% phosphoric acid was added. The samples were allowed to react at 60 C for 1 h to overnight. Sample pressure was adjusted to 1 atm by allowing the sample to equilibrate with a helium-filled syringe connected through the vial septum. Evacuation, acid addition, and heated reaction were performed by the automated gas handling system developed by Roberts et al. [10].

Reference and process blank materials were not pretreated. Carbonate shell samples for the core comparison study were picked from a split core and cleaned by washing with distilled water and dried at 60 C. Shell samples were crushed and mixed, but not otherwise pretreated. The homogenized carbonates were sub-sampled for measurement by HGIS (15mg) and as graphite (10mg).

Normalizing standards were prepared by evacuating vials and then filling with a modern standard CO_2 using the automated gas handling system. Standards were adjusted to the same size as other samples by extracting an appropriate volume of CO_2 from the full vial and replacing with helium using a syringe. Process blank samples were prepared from powdered IAEA C1 or TIRI F, acidified in vials using the method above.

2.3. Measurement

The HGIS measurements were carried out on a modified 3MV Tandetron AMS system [1]. Measurement of a sample proceeded as follows: a clean sputter target cathode was rotated into position and the target was pre-cleaned by sputtering for 5 minutes or until cathode ¹²C⁻ current fell below 100 nA. The delivery needle was then transferred to the sample vial, which started gas delivery to the split and source. Ion current was allowed to stabilize for 30 s, at which point the data acquisition was started. Data was acquired in 10 blocks of 90 s each, for 15 min total acquisition time. The displacement helium was allowed to flow constantly during cathode cleaning and analysis, and the sample needle was inserted into a helium-filled vial between samples. Normalizing standards, blanks, and secondary standards were measured identically to unknowns. One target is used per gas sample. Total time for a measurement was 20–25 min including target pre-cleaning and changing samples. Graphite samples were prepared at NOSAMS and measured on the CFAMS system using standard procedures [14,15].

2.4. Data reduction

After acquisition, data reduction, normalization and blank correction result in a final fraction modern with error. First, each 90 s block was corrected for fractionation using the AMS $^{13/12}$ C measurement. Blocks that are more than 1.5 times the interquartile range (IQR) below the first quartile of all measurements of

a sample or more than 1.5 IQR above the third quartile are considered outliers and were not further used in the analysis. Remaining blocks of a sample were averaged and sample uncertainty was taken as the greater of counting error or the standard error of the measurements. The sample ratio was then normalized using the mean of gas standards measured during the measurement session. The measurement error of the standards was taken as the greater of the standard error of all standards or the errors of the standards added in quadrature.

Measurements were corrected for process and measurement blank using a linear correction that assumes that the corrected ratio of blank samples should be zero, samples with the same ratio as the standard need no correction, and samples of intermediate ratio need a proportional correction (Equation 2) [16,17]. The correction uses measured values of standard gas and blank samples for correction of contaminant carbon and machine blank. The errors in the blanks and standards were propagated with errors of the samples to produce the final error estimate for the sample. For all measurements used to assess the precision and accuracy of the method, sample, standard, and blank masses were kept constant. Data were reduced using a package written in R [18] which is published on github (https://github.com/blongworth/hgis).

3. Results and Discussion

3.1. Source performance

Initial work with the NEC source established optimal source parameters for consistent source performance. We used tank CO_2 connected through a regulator and glass capillary to the ion source to measure source performance over a range of CO_2 flows. Best $^{12}C^-$ ion current for the source was 10 μ A, or roughly 10% of typical graphite target current. Peak current was produced at a CO_2 flow rate of 7.5 μ l min⁻¹ CO_2 , but the source produced near optimal currents with flows from 7.5–25 μ l min⁻¹ CO_2 . This is comparable with other hybrid sources [2], although improved target design and continued optimization of source parameters may improve performance [3,7,19]. Typical currents for this study were 4–9 μ A and average current for all samples was 6.3 \pm 1.6 μ A. Several studies have shown best currents at lower CO_2 flow rates [2,12].

Source ion currents are variable by day and by target under similar source, inlet, and sample conditions. Factors affecting source current may include capillary condition, source and gas delivery arm alignment, slight variability in target geometry, source condition, and performance of the ionizer and cesium reservoir. Capillary clogging caused occasional flow issues, especially when sampling from vials containing acid.

A contrast of the open split approach with closed-source HGIS methods is changing CO_2 flow and helium dilution ratio over the period of measurement due to the dilution of the sample by the displacement helium. We examined the effect of this variable carbon delivery and dilution by measuring $^{12}C^-$ current (Figure 2a) and 14/12 C ratio (Figure 2b) evolution during helium displacement/dilution of vial CO_2 and comparing this to the composition of the gas delivered to the source. We estimated gas composition (Figure 2c) using a simple mixing model:

$$C(t) = e^{-\frac{r}{V}t} \tag{1}$$

Where C(t) is the fraction CO_2 at time t, r is the rate of helium displacement flow, and V is the initial volume of the CO_2 -filled vial. Figure 3 shows the resulting relationship of sample ion current to CO_2 flow rate. The most important feature of the current-flow relationship is the wide range of CO_2 flow rates over which stable ion current is measured, which in turn produces relatively stable currents and ratios despite a changing carbon flow rate during measurement. Several studies have measured peak currents over a narrower range of flows [7,19] at high helium dilution rates (> 90% helium), while Xu et al. [2] shows a somewhat wider flow range producing high currents with pure CO_2 . Brock et al. [19] found that the range of flow rates with peak currents increased with decreasing dilution ratio. While lower rates of dilution used in our HGIS method may decrease current slightly, the observed relationship between ion current and flow rate allows stable measurement over the range of CO_2 flows produced by the open split.

Work with currents and flows (above and Figure 2) shows that stable currents are produced until less than 2 ml CO_2 (0.8 mg C) remains in the sample vial. Tests of a range of sample sizes support this estimate and show that no reduction in measured current is seen in samples larger than 1 mg C which corresponds to

 8 mg CaCO_3 sample material. To ensure sufficient sample for optimal measurements, we chose 15 mg as a target sample mass. We allowed samples to equilibrate to 1 atm pressure using a syringe filled with helium when the reaction with acid was complete.

3.2. Contaminant carbon

The HGIS method produced higher $^{14/12}C$ ratios for radiocarbon dead samples than the graphite method. The average uncorrected $F^{14}C$ for radiocarbon-free reference materials IAEA C1 marble and TIRI F spar calcite was 0.016 ± 0.007 (1σ uncertainty, N=21), compared to 0.003 ± 0.001 for these materials run as graphite on the CFAMS system. We investigated the sources of this method blank as a current-dependent blank and as a current-independent blank, and implemented a blank correction for the method.

HGIS cathodes produce measurable ion current, even with no gas flow. This current was initially > 10 μ A and dropped exponentially, reaching a baseline of ~100 nA after 5-10 minutes. For the range of currents in this study (3–9 μ A), this baseline current represents a 1–6% contribution to the total measured sample current at the F¹⁴C of the target current baseline. This can be interpreted as a constant current dependent blank, analogous to a mass-dependent "constant contaminant" blank and may be modeled with the same tools [17,20–22]. To assess blank contribution and ratio dependence on sample current, vials of live and dead standard gas were measured as the displacement helium flow diluted the samples, producing diminishing current over time. We used these data to develop a current-balance model following methods used to assess mass-dependent or constant contamination blanks in graphite targets [22,23]. The constant contamination blank was also assessed directly by measuring pure helium in vials using the same method. Results from both tests are shown in Figure 4a. The inverse of the sample current is used to linearize the data, allowing assessment with a simple linear model. Fits from modern and dead dilution tests should trend towards the fraction modern of the blank, crossing at the inverse of blank current. Based on this assessment, we estimate the F¹⁴C of the blank as 0.43 with a current of 110 nA.

The directly measured blank current (120 nA) agrees well with the model assessment, but has higher $F^{14}C$ (0.82). A combination of low measurement precision for the direct measurement and high sensitivity of the model to variability in the measured fraction modern and current in the depletion samples may explain this difference [22]. This constant contamination blank is consistent with the fact that hybrid cathodes produce a minimum current with or without gas flow to the source. Given that this blank cathode current is a significant fraction of measured sample current, this current likely makes up a large fraction of the method blank.

While dilution and direct measurement data show evidence for a constant blank with a variable effect depending on sample size, the blank correction may be simplified if blanks, standards, and unknown samples are the same size [16,17]. If the fraction modern of the blank is 0.8 modern as estimated above, radiocarbon-free samples will show the most effect of a constant contamination blank with current. Figure 4b shows the fraction modern of measured blanks compared to their mean ¹²C⁻ ion current. Fraction modern of measured blanks does decrease with increasing current, but the decrease is small, less than F¹⁴C 0.01 over the range of currents measured. This change with current is roughly equal to the variability between blanks, so the error due to the use of a current-dependent blank based on samples measured over multiple measurement sessions will likely be larger than a current independent blank correction based on blanks measured during each session. Constant current blank is likely the best model, but we simplify to a linear correction based on the measured ratio of process blanks and normalizing standards:

$$R_{samp} = R_{meas} - \frac{R_{blank}(R_{std} - R_{meas})}{R_{std}}$$
 (2)

where R_{samp} is the ratio of the unknown sample, R_{meas} is the measured ratio, R_{blank} is the ratio of the blank, and R_{std} is the ratio of the normalizing standard. This mass-independent blank correction works well for our data since blanks vary by run and ion currents are relatively similar between blanks, unknowns and standards.

3.3. Standard reference materials

Precision and accuracy of the method were assessed by measuring carbonate reference standards for comparison with consensus values from graphite measurements. We measured TIRI I, a roughly quarter-modern turbidite carbonate, IAEA C2, a half modern travertine, and NOSAMS 2, a modern bivalve mollusk internal standard. Summary data for these samples are given in Table 1, and measurement data for all samples is in supplementary information. Measurement, data reduction, and blank correction was performed as described above.

Reference materials analyzed with the hybrid gas method were in good agreement with consensus values. Mean difference from consensus for all measurements was $F^{14}C$ -0.0004 shows that the hybrid method has no bias in aggregate. The standard deviation of the difference in $F^{14}C$ was 0.0110, which may be taken as an estimate of the 1σ precision of the method. The mean of propagated measurement errors for these samples was 0.0113 $F^{14}C$ for these samples, which is in good agreement with the method precision above. The method error is about three times larger than the 2–3 ‰ precision of graphite measurements, but is within the range of method precision of other gas sources.

The difference between reference samples and graphite consensus does not vary systematically by F¹⁴C, indicating that the method has no significant bias with radiocarbon content (Figure 5). Each reference standard type agrees with graphite consensus values within the standard deviation of samples measured, with slightly more measurements agreeing with graphite within 1σ uncertainties than would be expected statistically.

3.4. Carbonate macrofossils for age-depth model

A suite of 15 carbonate macrofossils consisting of shell and coral fragments from a series of coastal marine cores [24] were measured as graphite and as CO₂ using the HGIS method to further test the method and serve to demonstrate a potential application. Sediment cores were collected from Baie des Baradères, Haiti in May 2016. Coring was performed with a Rossfelder vibracorer from a 20-foot pontoon boat. The cores were collected from a coastal karst basin at vertical depth ~11.7 m and coordinates 18.514° N, 73.629° W. Core HATC1 D1 is 145 cm long and was collected in a 3-inch poly tube as a control directly beside core HATC1 D2, which is a continuous 896 cm core collected in a 3-inch aluminum tube.

Carbonate materials such as corals and bivalve shells were selected throughout the core for the age-depth model, processed and measured as described above. Parallel graphite measurements were made following standard NOSAMS methods. One HGIS sample vial was noted to be at atmospheric pressure when the 16 mg sample should have produced only 0.5 atmosphere of $\rm CO_2$. The HGIS measurement for this sample was 0.053 $\rm F^{14}C$ higher than the measurement as graphite. We suspect that this sample was improperly sealed and eliminated it from the analysis as an outlier.

We found the HGIS and graphite measurements to be in good agreement, with no significant bias over the range in $F^{14}C$ of the core samples (0.4 to 1.15) (Figure 6a). Mean difference between hybrid and graphite measurements was -0.003 $F^{14}C$ and the standard deviation of this difference was 0.009 $F^{14}C$. Mean per-sample 1σ uncertainty was 0.010 $F^{14}C$ for HGIS measurements, compared with 0.002 $F^{14}C$ for graphite. Three samples were analysed by HGIS in duplicate. Two of the three pairs agreed within 1σ and all three agreed within 2σ .

Age models were developed for both the HGIS measurements (Figure 6b) and the traditional graphite measurements (Figure 6c) of the core carbonates. We used the Bchron Bayesian radiocarbon chronology package [25] to develop these models. We applied a correction for the regional marine reservoir effect with a Δ R of -216 \pm 92 years based on the Oxcal model [26] with 10 reservoir points. Samples with pre-bomb radiocarbon ages were calibrated using the Marine20 curve [27]. The NH zone 2 curve from Hua et al. [28] was used for calibration of postmodern dates, but these measurements were not included in the age model due to uncertainties in reservoir correction. The age-depth curves produced by the two datasets agree within the uncertainty of the chronologies (Figure 6d & 6e), with the largest differences being in the uncertainty of the individual dates.

4. Conclusions

We developed a method for the analysis of carbonates using an open-split interface to a hybrid sputter gas ion source. This system produces results that agree with graphite measurements within the approximately 1% method error from 8–20 mg of carbonate. Sample preparation takes about 10 min of person time and 1 h of automated processing and reaction time, and 20 min of measurement time per sample. The simplicity of of this approach can potentially reduce sample cost by eliminating graphitization, and may improve reliability and reduce maintenance compared to more complex sample inlet designs. Further development should focus on improvement of precision and accuracy by increasing currents and current stability and reducing the magnitude and uncertainty of the blank.

With lower cost and time per sample, the lower precision of the method may be balanced by the ability to measure more samples from a population, i.e. triplicate measurement or more core depths. This may lead to more accurate results compared to a more precise graphite measurement where reproducibility is not well constrained by multiple measurements. The accuracy of age-depth models is often limited by environmental factors and sparse data, rather than the precision of individual dates [29]. The lower time and cost of the hybrid method allows analysis of more samples. This may produce more accurate age models, despite reduced precision of individual measurements.

Acknowledgements

This work was supported by the NOSAMS NSF cooperative agreement 1755125. S. Pendleton was supported by a WHOI/NOSAMS Postdoctoral fellowship. We are grateful to K. von Reden, A. Gagnon, K. Gospodinova, and J. Hlavenka for initial work and discussions on the NOSAMS HGIS; C. McIntyre, T. Broek, G. Salazar, and T. Ognibene for discussions on gas handling and gas ion sourcery; J. Gunnard and T. Broek for improvements to the text; and the staff of NOSAMS for assistance with the HGIS and preparation of graphite samples.

Figures

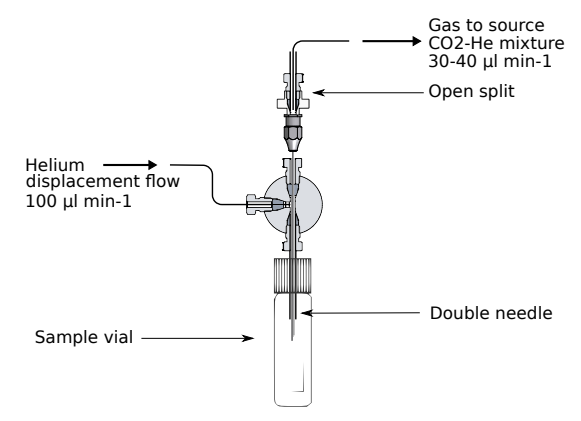


Figure 1: Schematic of the open split inlet. The double needle is housed in a tee fitting and allows displacement helium to flow into the sample vial and the sample-helium mixture to flow to the open split, where a capillary delivers the mixture to the ion source.

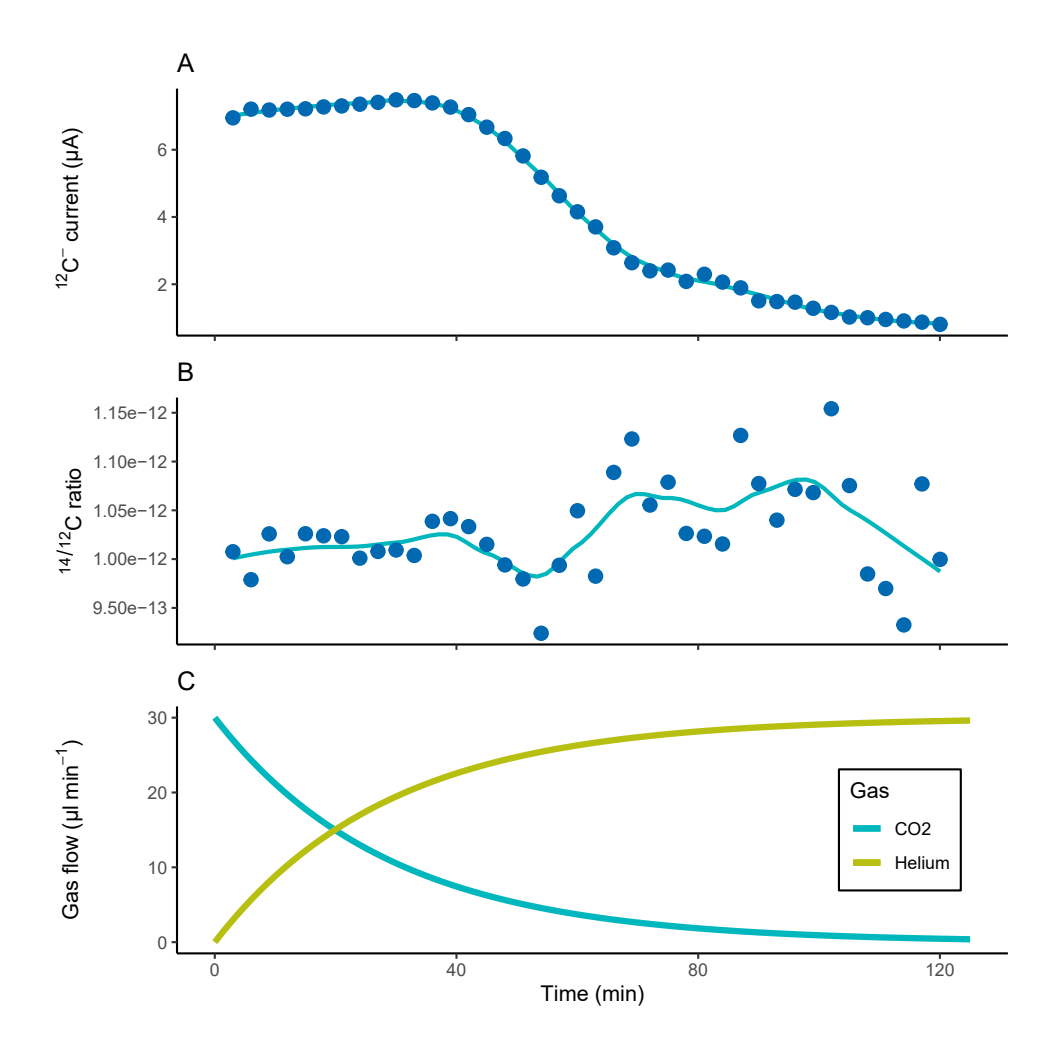


Figure 2: Performance of the NOSAMS MCSNICS hybrid gas ion source. (a) Measured $^{12}C^-$ ion current during displacement of modern tank CO_2 from a sample vial with helium. (b) Uncorrected $^{14/12}C$ ratio measured during the same test. (c) Modeled flows of helium and CO_2 to the ion source during the same dilution experiment.

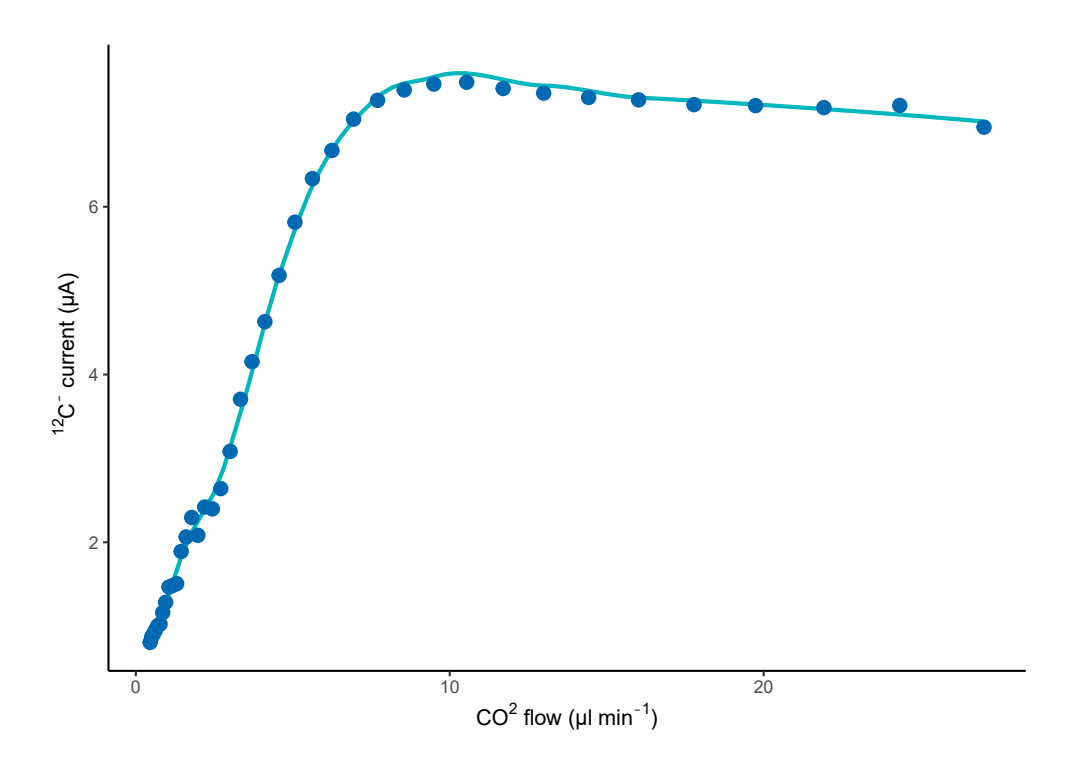


Figure 3: Measured ion current for the modeled CO_2 flow using the same data as figure 2. The stability of the source over a range of flow produces stable current for up to 40 min of measurement time.

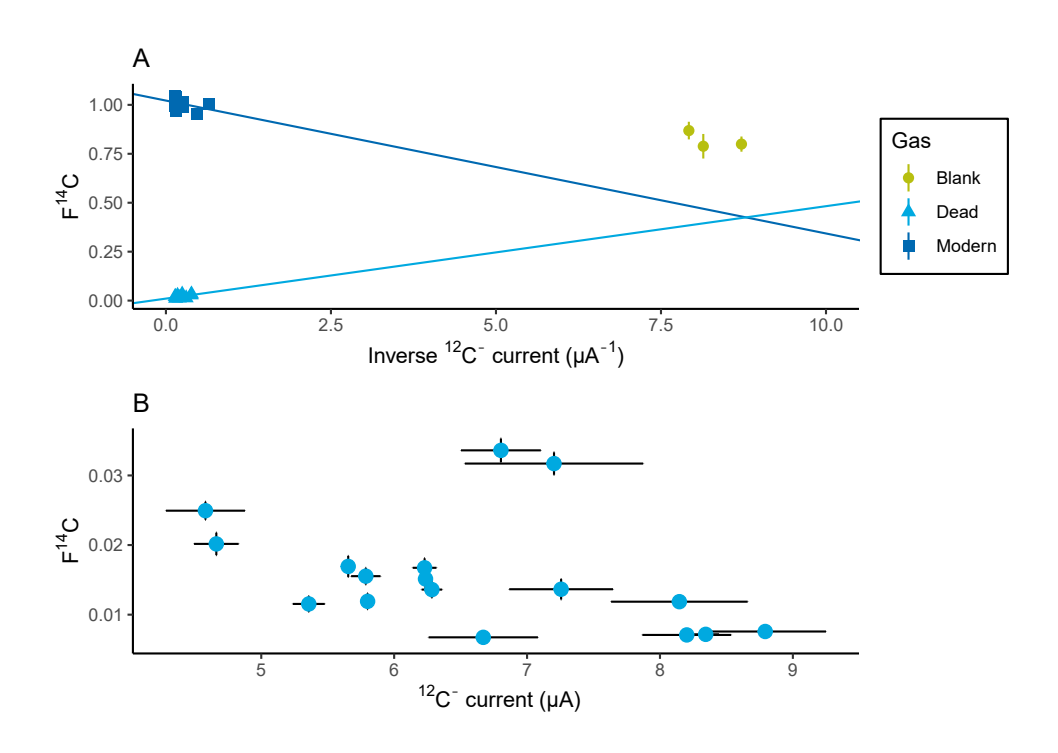


Figure 4: Assessment of blanks. (a) Current dependent blank model and data. $F^{14}C$ and current of measurements from dilution tests of modern and dead tank standards are used to generate linear fits which should cross at the $F^{14}C$ and current of the constant current blank. Direct determination of $F^{14}C$ and current of the blank using clean targets and helium without CO_2 are also shown. (b) Fraction modern of large IAEA C1 and TIRI F carbonate blank samples compared to sample current. Horizontal and vertical bars represent measurement uncertainty in current and ratio, respectively.

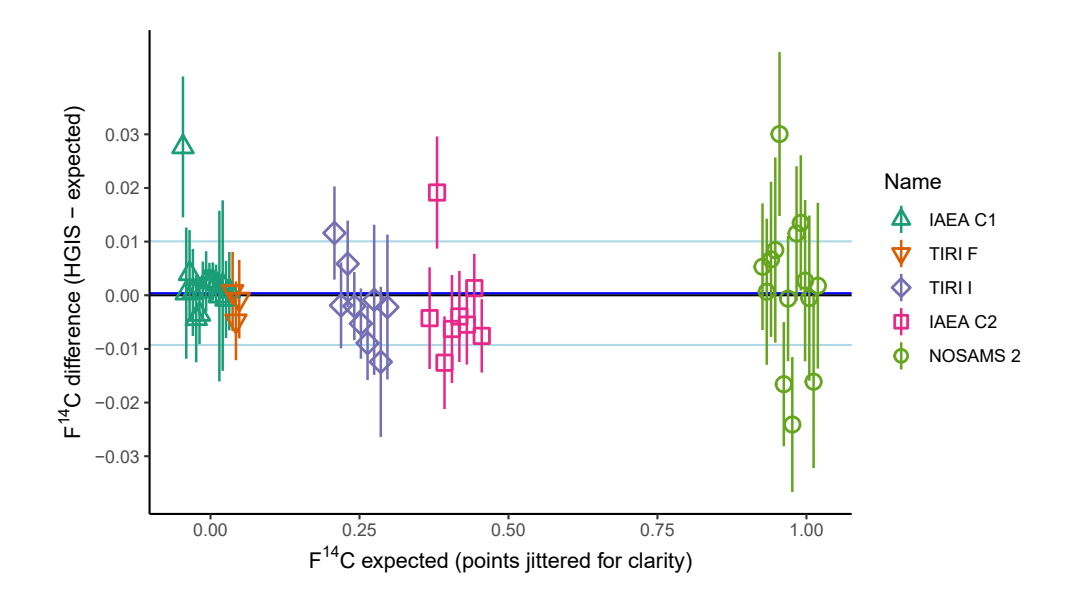


Figure 5: Agreement of standards with graphite consensus values. Difference of HGIS measurements from consensus for individual samples are plotted against their expected value. Expected values are spread to avoid overlapping points. Error bars represent 1σ sample uncertainty. The black line is the mean difference from expected value for all measurements, and the blue lines are one standard deviation of all measurements.

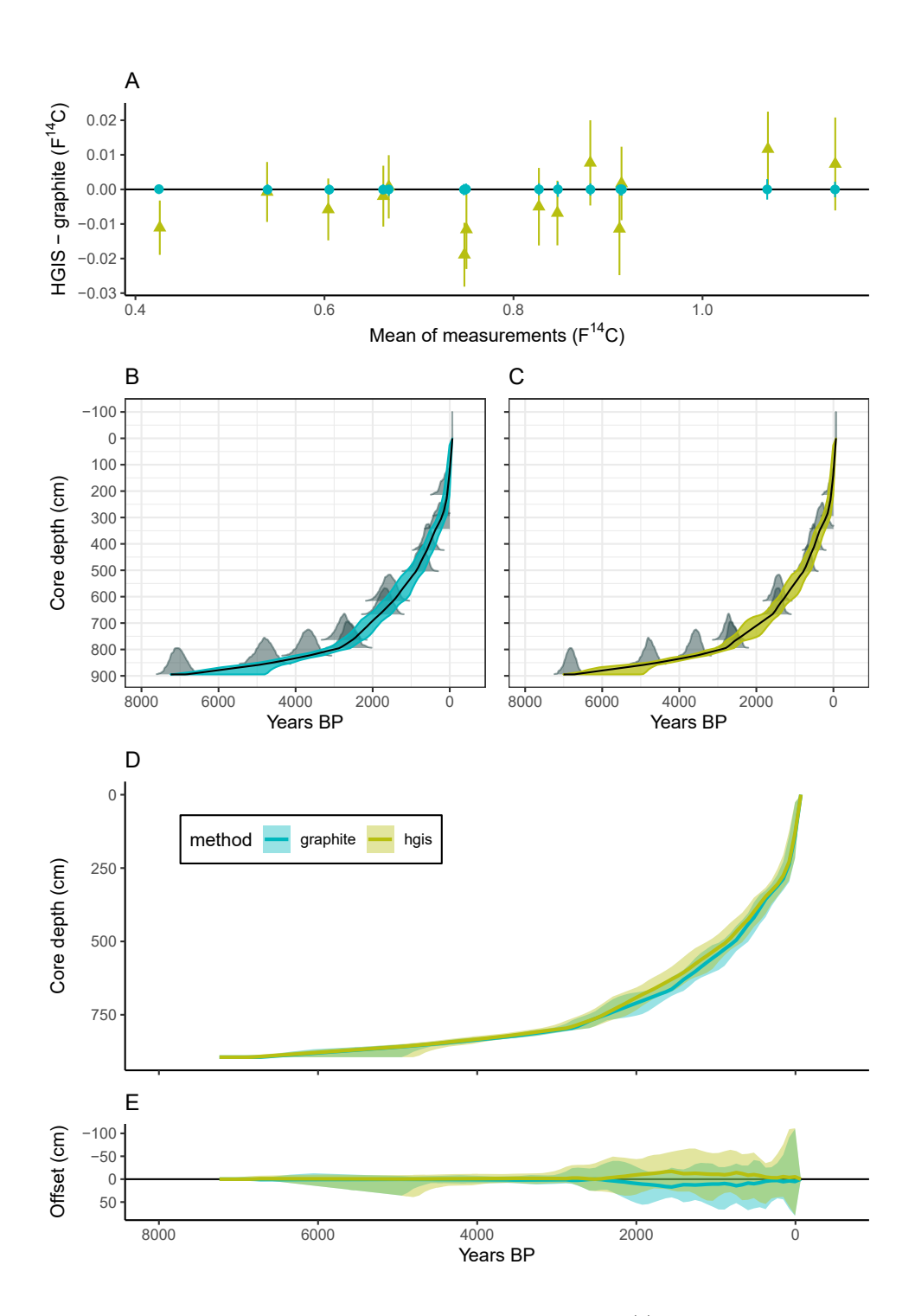


Figure 6: Comparison of Haiti core samples measured as graphite and via HGIS. (a) Difference between HGIS and graphite measurements of the same materials. Difference between HGIS and graphite measurements is shown on the vertical axis and plotted against the mean of the two measurements. Error bars are 1σ measurement uncertainty for each sample. Graphite measurements are included to allow comparison of uncertainty. Bayesian age-depth models produced using HGIS (b) and graphite measurements (c). Grey subplots show probability distribution of calibrated ages. (d) Combined age-depth prediction and 95% confidence intervals for HGIS and graphte. (e) Offset of HGIS and graphite values from the mean of the models with confidence intervals.

Tables

Table 1: Reference material precision and accuracy. Reference values are community consensus values for TIRI I and C2, and the NOSAMS internal graphite value for NOSAMS2. The mean of per-sample error estimates is included for comparison to the reproducibilty of the samples.

Sample Name	Reference F ¹⁴ C	HGIS $F^{14}C \pm stdev$	Mean per-sample error	N
TIRI I	0.2524	0.251 ± 0.007	0.010	9
IAEA C2	0.4114	0.41 ± 0.01	0.008	8
NOSAMS 2	0.9727	0.97 ± 0.01	0.014	14

Supplementary Materials

Table 2: Measurements of reference standard materials. Reference values are community consensus values for TIRI I and C2, and the NOSAMS internal graphite value for NOSAMS2.

Sample Name	Reference F ¹⁴ C	HGIS $F^{14}C \pm 1\sigma$	$^{12}\text{C}^{\text{-}} \text{ current } (\mu\text{A})$
IAEA C1	0.0002	0.03 ± 0.01	4.1
IAEA C1	0.0002	0.00 ± 0.01	4.6
IAEA C1	0.0002	0.004 ± 0.008	4.7
IAEA C1	0.0002	0.001 ± 0.008	6.2
IAEA C1	0.0002	-0.004 ± 0.008	5.8
IAEA C1	0.0002	-0.003 ± 0.006	8.8
IAEA C1	0.0002	0.001 ± 0.006	8.1
IAEA C1	0.0002	0.003 ± 0.006	7.3
IAEA C1	0.0002	0.003 ± 0.004	8.2
IAEA C1	0.0002	0.003 ± 0.004	8.3
IAEA C1	0.0002	0.002 ± 0.004	6.7
IAEA C1	0.0002	0.00 ± 0.02	7.2
IAEA C1	0.0002	0.00 ± 0.02	6.8
IAEA C1	0.0002	-0.001 ± 0.007	6.3
IAEA C1	0.0002	0.001 ± 0.007	6.2
TIRI F	0.0018	0.003 ± 0.007	5.7
TIRI F	0.0018	-0.003 ± 0.007	5.4
TIRI F	0.0018	0.001 ± 0.007	5.8
TIRI I	0.2524	0.264 ± 0.009	6.3
TIRI I	0.2524	0.251 ± 0.008	5.7
TIRI I	0.2524	0.258 ± 0.008	6.0
TIRI I	0.2524	0.250 ± 0.006	8.6
TIRI I	0.2524	0.247 ± 0.007	7.3
TIRI I	0.2524	0.243 ± 0.007	6.8
TIRI I	0.2524	0.25 ± 0.01	3.7
TIRI I	0.2524	0.24 ± 0.01	3.8
TIRI I	0.2524	0.25 ± 0.01	5.1
IAEA C2	0.4114	0.407 ± 0.009	5.2
IAEA C2	0.4114	0.43 ± 0.01	3.4
IAEA C2	0.4114	0.399 ± 0.009	6.1
IAEA C2	0.4114	0.41 ± 0.01	6.4
IAEA C2	0.4114	0.407 ± 0.008	6.0
IAEA C2	0.4114	0.406 ± 0.007	8.0
IAEA C2	0.4114	0.413 ± 0.006	7.7
IAEA C2	0.4114	0.404 ± 0.007	6.3
NOSAMS 2	0.9727	0.98 ± 0.01	5.3
NOSAMS 2	0.9727	0.97 ± 0.01	3.3
NOSAMS 2	0.9727	0.98 ± 0.01	6.5
NOSAMS 2	0.9727	0.98 ± 0.02	5.0
NOSAMS 2	0.9727	1.00 ± 0.02	5.4
NOSAMS 2	0.9727	0.96 ± 0.01	6.7
NOSAMS 2	0.9727	0.97 ± 0.01	6.3
NOSAMS 2	0.9727	0.95 ± 0.01	6.7

Sample Name	Reference F ¹⁴ C	HGIS $F^{14}C \pm 1\sigma$	^{12}C - current (μA)
NOSAMS 2	0.9727	0.98 ± 0.01	7.7
NOSAMS 2	0.9727	0.99 ± 0.01	7.5
NOSAMS 2	0.9727	0.98 ± 0.02	6.3
NOSAMS 2	0.9727	0.97 ± 0.02	3.4
NOSAMS 2	0.9727	0.96 ± 0.02	4.8
NOSAMS 2	0.9727	0.97 ± 0.02	3.4

Table 3: HGIS and graphite measurements of Haiti core carbonates. HGIS replicates are listed without a corresponding graphite value.

Sample Name	Core Depth	HGIS $F^{14}C \pm 1\sigma$	graphite $F^{14}C \pm 1\sigma$
1:1_12-13	12.5	1.07 ± 0.01	1.063 ± 0.003
1:1_81_82	81.5	1.14 ± 0.01	1.136 ± 0.002
2:7_90-91	214.5	0.91 ± 0.01	0.922 ± 0.002
HATC1-D2_2:7	214.5	0.91 ± 0.01	$NA \pm NA$
3:7_25-26	294.5	0.92 ± 0.01	0.914 ± 0.002
3:7_73-74	343.5	0.89 ± 0.01	0.878 ± 0.002
4:7_10-11	424.5	0.843 ± 0.009	0.850 ± 0.002
4:7_95-96	504.5	0.82 ± 0.01	0.830 ± 0.002
5:7_57-58	616.5	0.74 ± 0.01	0.756 ± 0.002
5:7_108-109	667.5	0.735 ± 0.009	0.754 ± 0.002
HATC1-D2_5:7	667.5	0.75 ± 0.01	$NA \pm NA$
6:7_39-40	743.5	0.747 ± 0.009	0.695 ± 0.002
6:7_60-61	764.5	0.661 ± 0.009	0.663 ± 0.002
6:7_90-91	794.5	0.669 ± 0.009	0.668 ± 0.002
6:7_120-121	824.5	0.600 ± 0.009	0.606 ± 0.001
HATC1-D2_6:7	824.5	0.607 ± 0.008	$NA \pm NA$
7:7_8-9	855.5	0.539 ± 0.009	0.540 ± 0.002
7:7_47-48	894.5	0.420 ± 0.008	0.431 ± 0.001

References

- [1] B.E. Longworth, K.F. von Reden, P. Long, M.L. Roberts, A high output, large acceptance injector for the NOSAMS tandetron AMS system, Nuclear Instruments and Methods in Physics Research Section B: Beam Interactions with Materials and Atoms. 361 (2015) 211–216. https://doi.org/10.1016/j.nimb.2015.04.005.
- [2] S. Xu, A. Dougans, S.P.H.T.H.T. Freeman, C. Maden, R. Loger, A gas ion source for radiocarbon measurement at SUERC, Nuclear Instruments and Methods in Physics Research Section B: Beam Interactions with Materials and Atoms. 259 (2007) 76–82. https://doi.org/10.1016/j.nimb.2007.01.311.
- [3] G. Salazar, T. Ognibene, Design of a secondary ionization target for direct production of a c— beam from CO2 pulses for online AMS, Nuclear Instruments and Methods in Physics Research Section B: Beam Interactions with Materials and Atoms. 294 (2013) 300–306. https://doi.org/10.1016/j.nimb.2012.03.039.
- [4] T. Uhl, W. Luppold, A. Rottenbach, A. Scharf, K. Kritzler, W. Kretschmer, Development of an automatic gas handling system for microscale AMS 14C measurements, Nuclear Instruments and Methods in Physics Research, Section B: Beam Interactions with Materials and Atoms. 259 (2007) 303–307. https://doi.org/10.1016/j.nimb.2007.01.173.
- [5] M. Ruff, L. Wacker, H.W. Gäggeler, M. Suter, H.-A. Synal, S. Szidat, A gas ion source for radiocarbon measurements at 200 kV, Radiocarbon. 49 (2007) 307–314. https://doi.org/10.1017/S0033822200042235.
- [6] M. Ruff, S. Fahrni, H.W. Gäggeler, I. Hajdas, M. Suter, H.-A. Synal, S. Szidat, L. Wacker, On-line radiocarbon measurements of small samples using elemental analyzer and MICADAS gas ion source, Radiocarbon. 52 (2010) 1645–1656. https://doi.org/10.1017/S003382220005637X.
- [7] S.M. Fahrni, L. Wacker, H.-A. Synal, S. Szidat, Improving a gas ion source for 14C AMS, Nuclear Instruments and Methods in Physics Research Section B: Beam Interactions with Materials and Atoms. 294 (2013) 320–327. https://doi.org/10.1016/j.nimb.2012.03.037.
- [8] L. Wacker, S.M. Fahrni, I. Hajdas, M. Molnar, H.-A. Synal, S. Szidat, Y.L. Zhang, A versatile gas interface for routine radiocarbon analysis with a gas ion source, Nuclear Instruments and Methods in Physics Research Section B: Beam Interactions with Materials and Atoms. 294 (2013) 315–319. https://doi.org/10.1016/j.nimb.2012.02.009.
- [9] J. Gottschalk, S. Szidat, E. Michel, A. Mazaud, G. Salazar, M. Battaglia, J. Lippold, S.L. Jaccard, Radiocarbon measurements of small-size foraminiferal samples with the mini carbon dating system (MICADAS) at the university of bern: Implications for paleoclimate reconstructions, Radiocarbon. 60 (2018) 469–491. https://doi.org/10.1017/RDC.2018.3.
- [10] M.L. Roberts, S.R. Beaupré, J.R. Burton, A high-throughput, low-cost method for analysis of carbonate samples for 14C, Radiocarbon. 55 (2013) 585–592. https://doi.org/10.2458/azu_js_rc.55.16190.
- [11] G. Salazar, S. Szidat, A low-cost continuous-flow gas interface for coupling an elemental analyzer with a micadas AMS: Gas flow mathematical model and first results, Radiocarbon. 61 (2019) 1795–1804. https://doi.org/10.1017/RDC.2019.93.
- [12] M. Ruff, S. Szidat, H.W. Gäggeler, M. Suter, H.A. Synal, L. Wacker, Gaseous radiocarbon measurements of small samples, Nuclear Instruments and Methods in Physics Research, Section B: Beam Interactions with Materials and Atoms. 268 (2010) 790–794. https://doi.org/10.1016/j.nimb.2009.10.032.
- [13] C. Bronk Ramsey, P. Ditchfield, M. Humm, Using a gas ion source for radiocarbon AMS and GC-AMS, Radiocarbon. 46 (2004) 25–32. https://doi.org/10.1017/S003382220003931X.
- [14] A.R. Gagnon, A.P. McNichol, J.C. Donoghue, D.R. Stuart, K. von Reden, The NOSAMS sample preparation laboratory in the next millenium: Progress after the WOCE program, Nuclear Instruments and Methods in Physics Research Section B: Beam Interactions with Materials and Atoms. 172 (2000) 409–415. https://doi.org/10.1016/S0168-583X(00)00201-9.

- [15] M.L. Roberts, J.R. Burton, K.L. Elder, B.E. Longworth, C.P. McIntyre, K.F. von Reden, B.X. Han, B.E. Rosenheim, W.J. Jenkins, E. Galutschek, A.P. McNichol, A high-performance ¹⁴ c accelerator mass spectrometry system, Radiocarbon. 52 (2010) 228–235. https://doi.org/10.1017/S0033822200045252.
- [16] D.J. Donahue, T.W. Linick, A.J.T. Jull, Isotope-ratio and background corrections for accelerator mass spectrometry radiocarbon measurements, Radiocarbon. 32 (1990) 135–142. https://doi.org/10.1017/S0033822200040121.
- [17] M.L. Roberts, K.L. Elder, W.J. Jenkins, A.R. Gagnon, L. Xu, J.D. Hlavenka, B.E. Longworth, 14C blank corrections for 25–100 g samples at the national ocean sciences ams laboratory, Radiocarbon. 61 (2019) 1–9. https://doi.org/10.1017/rdc.2019.74.
- [18] R Core Team, R: A language and environment for statistical computing, R Foundation for Statistical Computing, Vienna, Austria, 2022. https://www.R-project.org/.
- [19] T.A.B. Broek, K.C. Moreland, T.J. Ognibene, K.J. McFarlane, T.A. Brown, Optimization of the LLNL-CAMS gas accepting ion source and 1 MV compact AMS for natural abundance radiocarbon analysis, Nuclear Instruments and Methods in Physics Research Section B: Beam Interactions with Materials and Atoms. (n.d.).
- [20] N. Haghipour, B. Ausin, M.O. Usman, N. Ishikawa, L. Wacker, C. Welte, K. Ueda, T.I. Eglinton, Compound-specific radiocarbon analysis by elemental analyzer–accelerator mass spectrometry: Precision and limitations, Anal. Chem. 91 (2019) 2042–2049. https://doi.org/10.1021/acs.analchem.8b04491.
- [21] U.M. Hanke, L. Wacker, N. Haghipour, M.W.I. Schmidt, T.I. Eglinton, C.P. McIntyre, Comprehensive radiocarbon analysis of benzene polycarboxylic acids (BPCAs) derived from pyrogenic carbon in environmental samples, Radiocarbon. 59 (2017) 1103–1116. https://doi.org/10.1017/RDC.2017.44.
- [22] S. Sun, V.D. Meyer, A.M. Dolman, M. Winterfeld, J. Hefter, W. Dummann, C. McIntyre, D.B. Montluçon, N. Haghipour, L. Wacker, T. Gentz, T.S. van der Voort, T.I. Eglinton, G. Mollenhauer, ¹⁴ c blank assessment in small-scale compound-specific radiocarbon analysis of lipid biomarkers and lignin phenols, Radiocarbon. 62 (2020) 207–218. https://doi.org/10.1017/RDC.2019.108.
- [23] S.R. Shah Walter, A.R. Gagnon, M.L. Roberts, A.P. McNichol, M.C.L. Gaylord, E. Klein, Ultra-small graphitization reactors for ultra-microscale 14C analysis at the national ocean sciences accelerator mass spectrometry (NOSAMS) facility, Radiocarbon. 57 (2015) 109–122. https://doi.org/10.2458/azu_rc.57.18118.
- [24] S. Moser, Multi-proxy ~8500 year paleoenvironmental reconstruction of baie des baradères, haiti, PhD thesis, 2021. https://doi.org/10.20381/RUOR-27117.
- [25] J. Haslett, A. Parnell, A simple monotone process with application to radiocarbon-dated depth chronologies, Journal of the Royal Statistical Society: Series C (Applied Statistics). 57 (2008) 399–418. https://doi.org/10.1111/j.1467-9876.2008.00623.x.
- [26] C. Bronk Ramsey, Bayesian analysis of radiocarbon dates, Radiocarbon. 51 (2009) 337–360. https://doi.org/10.1017/S0033822200033865.
- [27] T.J. Heaton, P. Köhler, M. Butzin, E. Bard, R.W. Reimer, W.E.N. Austin, C. Bronk Ramsey, P.M. Grootes, K.A. Hughen, B. Kromer, P.J. Reimer, J. Adkins, A. Burke, M.S. Cook, J. Olsen, L.C. Skinner, Marine 20—the marine radiocarbon age calibration curve (0–55,000 cal BP), Radiocarbon. 62 (2020) 779–820. https://doi.org/10.1017/RDC.2020.68.
- [28] Q. Hua, M. Barbetti, A.Z. Rakowski, Atmospheric radiocarbon for the period 1950–2010, Radiocarbon. 55 (2013) 2059–2072. https://doi.org/10.2458/azu_js_rc.v55i2.16177.
- [29] M. Blaauw, J.A. Christen, K.D. Bennett, P.J. Reimer, Double the dates and go for bayes impacts of model choice, dating density and quality on chronologies, Quaternary Science Reviews. 188 (2018) 58–66. https://doi.org/10.1016/j.quascirev.2018.03.032.